

# Behavior of Saline Ice under Cyclic Flexural Loading

Andrii Murdza<sup>1</sup>, Erland M. Schulson<sup>1</sup>, Carl E. Renshaw<sup>1,2</sup>

<sup>1</sup>Thayer School of Engineering, Dartmouth College, Hanover, NH, USA, 03755

<sup>2</sup>Department of Earth Sciences, Dartmouth College, Hanover, NH, USA, 03755

*Correspondence to:* Andrii Murdza (Andrii.Murdza@dartmouth.edu)

**Abstract.** New systematic experiments reveal that the flexural strength of saline S2 columnar-grained ice loaded normal to the columns can be increased upon cyclic loading by about a factor of 1.5. The experiments were conducted using reversed cyclic loading over ranges of frequencies from 0.1 to 0.6 Hz and at a temperature of -10 °C on saline ice of two salinities: 3.0±0.9 and 5.9±0.6 ‰. Acoustic emission hit rate during cycling increases with an increase of stress amplitude of cycling. Flexural strength of saline ice of 3.0±0.9 ‰ salinity appears to increase linearly with increasing stress amplitude, similar to the behavior of laboratory-grown freshwater ice (Murdza et al., 2020b) and to the behavior of lake ice (Murdza et al., 2020a). The flexural strength of saline ice of 5.9±0.6 ‰ depends on the vertical location of the sample within the thickness of an ice puck; i.e., the strength of the upper layers, which have a lower brine content, was found to be as high as three times that of lower layers. The fatigue life of saline ice is erratic. Cyclic strengthening is attributed to the development of an internal back stress that opposes the applied stress and originates possibly from dislocation pileups.

## 1. Introduction

Fatigue of materials is a subject of practical importance in engineering and has been widely studied (Bathias and Pineau, 2013; Broek, 1986; Schijve, 2009; Suresh, 1998). Fatigue refers to changes in material properties resulting from cyclic loading. Fatigue strength of crystalline materials is typically controlled by microcrack initiation and subsequent growth that leads to failure.

It is not surprising that fatigue appears to play an important role in sea ice mechanics. For example, the Arctic and Antarctic floating ice covers and ice shelves are subjected to cyclic loading from ocean swells that can penetrate deeply into an ice pack and potentially result in the breakup of the ice cover (Squire, 2007). Such events, where under the action of surface waves a floating ice cover exhibited sudden breakup into smaller pieces, have been repeatedly witnessed and described (Shackleton, 1982; Liu and others, 1988; Prinsenber and Peterson, 2011; Asplin and others, 2012; Collins and others, 2015; Kohout and others, 2016; Hwang and others, 2017). Ice cover breakup leads to a decline in albedo (Pistone and others, 2014; Zhang and others, 2019) and to the acceleration of melting. Also, smaller ice floes attenuate ocean waves less effectively than does the parent solid ice cover, thereby endangering coastal zones to erosion. Given the retreat of the sea ice cover and the attendant increase in oceanic fetch, larger waves are expected to develop; correspondingly, the remaining ice cover is expected to be subjected to episodes of greater cyclic loading. The potential for fatigue failure is thus increasing.

34

35           Cyclic loading may also play an important role in other scenarios. For instance, during ice-structure  
36 interactions (Jordaan, 2001; Hendrikse and Metrikine, 2016; O'Rourke and others, 2016; Jordaan and others, 2008)  
37 the structure itself, such as a light-house, may be weakened or damaged to a degree that depends on the strength of  
38 the ice. Other examples are runways and roads that are built by freezing water on cold oceans, rivers and lakes and  
39 subsequently subject to cyclic loading. Therefore, it is important to understand the behavior of ice under cyclic  
40 loading.

41

42           Currently, the effects of cyclic loading on the physical and mechanical properties of sea ice and on the  
43 susceptibility of the material to fatigue are poorly constrained. Tabata and Nohguchi (1980) conducted experiments  
44 on sea ice sampled from Lake Saroma, Hokkaido, Japan and from Barrow, Alaska. They loaded the ice cyclically  
45 under uniaxial compression between two specified stress levels under a variety of combinations of strain rate (from  
46  $10^{-5} \text{ s}^{-1}$  to  $10^{-2} \text{ s}^{-1}$ ), temperature (from  $-2 \text{ }^{\circ}\text{C}$  to  $-24 \text{ }^{\circ}\text{C}$ ) and orientation (horizontal and vertical). They found that  
47 with a decrease of average stress and with a decrease of amplitude, the time to failure increases; and by lowering the  
48 temperature, the time to failure and the number of cycles also increases.

49

50           Other evidence of the weakening of sea ice under wave-driven in situ cyclic loading is discussed by  
51 Haskell and others (1996), Bond and Langhorne (1997), Langhorne and others (1998), (1999), (2001). In these  
52 works the authors obtained an S-N fatigue curve (S, upper peak stress of cycling; N, number of cycles imposed to  
53 failure), typical of curves obtained from engineering materials, i.e. for lower stress amplitude more cycles are  
54 needed for failure. The authors stated that the endurance limit, that is the stress amplitude below which the sea ice  
55 can withstand an unlimited number of cycles, is approximately one-half the failure stress of non-cycled ice.

56

57           The constitutive behavior of saline ice under cyclic loading was also investigated previously (Cole, 1995,  
58 1998; Cole et al., 1998, 2002; Cole and Dempsey, 2004; Cole and Durell, 1995; Dempsey et al., 2003; Wei et al.,  
59 2020); specifically, inelastic deformation of sea ice was explored and interpreted in terms of a dislocation-based  
60 mechanism. In these works the authors investigated the effect of temperature (from  $-5$  to  $-50 \text{ }^{\circ}\text{C}$ ), microstructure  
61 (total porosity varied from 14 to 104 ppt), cyclic stress amplitude (from 0.04 to 0.8 MPa), loading frequency (from  
62  $10^{-3}$  to 1 Hz), and dry isothermal vs floating specimens on the response of the ice. However, the strength of ice after  
63 it had been cycled was not measured.

64

65           Nothing more (to our knowledge) has been reported on the fatigue of sea ice. The topic is absent from a  
66 critical review by Squire (2007) and from two recent books on ice (Schulson and Duval, 2009; Weeks, 2010).

67

68           The behavior summarised above indicating the weakening of ice under cyclic loading, obtained from  
69 experiments conducted on saline and sea ice, might possibly account for the sudden breakup of natural ice covers.  
70 However, this behavior appears in conflict with the behavior of freshwater ice under cyclic loading (Cole, 1990;

71 Gupta et al., 1998; Iliescu et al., 2017; Iliescu and Schulson, 2002; Murdza et al., 2019, 2020b, 2020a). In those  
72 experiments, it was discovered that the ice flexural strength increases upon repetitive loading, followed by the  
73 recovery of the cyclic-induced increment in strength to the original non-cycled strength upon post-cycling annealing.  
74 This difference in the behavior of the two kinds of ice could perhaps be attributed to the presence of defects in  
75 sea/saline ice, such as brine pockets, brine channels and non-penetrating microcracks. Such defects serve as stress  
76 concentrators, thereby lessening the need to nucleate cracks to the degree that fatigue life may be governed primarily  
77 by crack propagation. The strengthening of ice is of more than scientific interest, reflected, perhaps in an interesting  
78 comment of an arctic engineer who reported that builders of ice roads never trust the ice until it had been “worked  
79 in” (Masterson, 2018).

80

81 Therefore, given that limited information about the behavior of sea/saline ice under cyclic loading and  
82 given the discrepancy in behavior of fresh and sea/saline ice, we conducted a study under controlled conditions in  
83 the laboratory on the flexural behavior of saline ice. In this paper, we describe the experiments in which beams of S2  
84 columnar-grained saline ice of two salinities ( $3.0 \pm 0.9$  and  $5.9 \pm 0.6$  ‰) were subjected at  $-10$  °C to four-point, reverse  
85 cycling at  $\sim 0.1$ - $0.6$  Hz and then, after several hundred or more cycles, were bent to failure, provided the beams did  
86 not break during cycling. We chose the rate of cycling to simulate the vibration frequency of a natural sea ice cover  
87 (Collins et al., 2015).

## 88 2. Experimental procedure

### 89 2.1 Ice growth and characterization

90 We studied saline ice of two melt-water salinities:  $3.0 \pm 0.9$  and  $5.9 \pm 0.6$  ppt, where  $\pm$  sign indicates standard  
91 deviation. We produced the ice in the laboratory in an 800 L circular polycarbonate tank in the manner described  
92 previously (Golding et al., 2014). Briefly, solutions containing  $17.5 \pm 0.2$  ppt and  $35 \pm 0.2$  ppt (parts per thousand,  
93 or ‰) of the commercial product “Instant Ocean” salt mixture were prepared and then frozen unidirectionally  
94 downward over a period of about 7 days by using a top-placed cold plate maintained at a temperature  $T = -$   
95  $20 \pm 0.1$  °C. Before bringing the cold plate into contact with the salt-water solution, the top surface of the solution  
96 was seeded with freshwater ice fragments of  $\sim 0.3$  - 1 mm in diameter. This procedure produced pucks  $\sim 1$  m in  
97 diameter and  $\sim 0.3$  m thick. For practical considerations, the bottom, skeletal layer of ice of about 7-10 cm was  
98 discarded as it was slushy and weak; we also believe that the skeletal layer does not play a significant role in  
99 supporting load. The top layer of ice of a few centimeters was also discarded because it was seeded and its grain size  
100 was considerably smaller and its microstructure thus different from the rest of the ice puck. Melt-water salinity was  
101 measured using a calibrated YSI Pro30 conductivity and salinity probe.

102

103 Figure 1 shows the microstructure of the ice. Table 1 lists its density and the average grain size of the test  
104 specimens described below. Figure 2 shows stereographic projections of the orientation of the crystallographic *c*-  
105 axes. The ice is characterized by columnar-shaped grains whose growth texture is marked by *c*-axes confined within

106 about 15° of the horizontal plane of the parent ice puck and randomly oriented within that plane. In other words, the  
107 ice is termed S2, after Michel and Ramseier (1971), and is similar to natural first-year sea ice (for comparison, see  
108 Figure 3.7 of Schulson and Duval (2009)). The grain size noted above is the average diameter of the columnar-shaped  
109 grains, ranging from about 2 to 7 mm in Figure 1.

## 110 **2.2. Growth features**

111 The ice contained both sub-mm sized brine pockets and supra-mm sized drainage channels, reminiscent of  
112 natural sea ice. Figures 3 and 4 show examples. The ice of lower salinity ( $3.0 \pm 0.9$  ppt) had fewer defects of both  
113 kinds. Some of the ice of higher salinity ( $5.9 \pm 0.6$  ppt) possessed channels whose size was almost as large as the  
114 grain diameter. The defects scattered light to the degree that in bulk form the ice had an overall opaque appearance.  
115 When observed in thin section ( $\sim 1$  mm) the ice exhibited to the naked eye distinct linear whitish features which we  
116 took to be sets of interconnected brine pockets that could possibly be filled with very fine-grained ice. The ice of  
117 higher salinity possessed more of these features, especially near the bottom of the parent puck (which was the last  
118 part to solidify). Our sense is that these features served as stress concentrators, particularly ones that traversed the  
119 width of the test specimen (described below), thereby weakening the ice. Indeed, as will become apparent, samples  
120 obtained from near the bottom of a puck of higher salinity ( $5.9 \pm 0.6$  ppt) had relatively low flexural strength.

121

122 Because the ice of both salinities exhibited a different appearance from the top and bottom of the parent  
123 puck, in preparing test specimens for flexing we distinguished them by their position (depth from top surface) within  
124 the ice puck from which they were prepared, Table 2.

## 125 **2.3. Sample preparation and test setup**

126 Once the ice had been grown, it was cut into blocks of dimensions  $\sim 10 \times 30 \times 20$  cm<sup>3</sup>, where the longest  
127 and the shortest dimensions are in the horizontal plane of the original ice puck, perpendicular to the direction of  
128 growth. The blocks were stored in a cooler (at  $-10 \pm 0.5$  °C) on their side (such that columnar-shaped grains were  
129 oriented horizontally) to reduce brine drainage for periods of time of about 1-10 weeks.

130

131 Specimens for flexing were manufactured from the ice blocks in the form of thin beams of dimensions  
132  $h \sim 16$  mm in thickness (parallel to the long axis of the grains),  $b \sim 85$  mm in width, and  $l \sim 300$  mm in length. The  
133 test specimens were allowed to equilibrate to the test temperature of  $-10 \pm 0.5$  °C for at least 24 hours before testing.

134

135 A detailed description of the specimens' preparation and loading can be found elsewhere (Iliescu et al.,  
136 2017; Murdza et al., 2018, 2019, 2020b). To summarize: The ice beams were flexed up and down under 4-point  
137 loading under constant displacement rate using a servo-hydraulic loading system (MTS model 810.14) to which we  
138 attached a custom-built 4-point loading frame, Figure 5. A load cell, calibrated for both tension and compression,  
139 and a linear variable differential transformer (LVDT) gauge were used for measurements of load and displacement  
140 of the upper surface of the ice beam during cycling.

141  
142  
143  
144  
145  
146  
147  
148  
149  
150  
151  
152  
153  
  
154  
155  
156  
157  
158  
159  
160  
161  
162  
163  
164  
165  
166  
167  
168  
169  
170  
171  
172  
173  
174  
175

Acoustic emissions were recorded during cycling using a PCI-2 18-bit A/D system; its frequency response was 3 kHz–3 MHz and its minimum acoustic emission (AE) amplitude detection threshold was set to 45 dB. We used a micro 30STC sensor (9.5 mm diameter, 11 mm thickness) which was attached to the top surface of an ice beam with a rubber band. Vacuum grease was used as the coupling agent between the sensor and the ice surface.

The experiments were performed in a cold room at a temperature of -10°C and at an outer-fiber center-point displacement rate of 0.1 mm s<sup>-1</sup> (or outer-fiber strain rate of about 1.4 x 10<sup>-4</sup> s<sup>-1</sup>). This displacement rate resulted in an outer-fiber stress rate in the range from ~ 0.3 to 0.5 MPa s<sup>-1</sup>, outer-fiber stress amplitude in the range from 0.35 to 1.2 MPa, outer-fiber strain amplitude in the range from ~ 1 to 5 x 10<sup>-4</sup> and frequencies in the range from 0.1 to 0.6 Hz (i.e. periods from ~10 to 1.5 sec). The period, as already noted, is similar to the period of ocean swells (Collins et al., 2015). The major outer-fiber stress  $\sigma_f$  was calculated from the relationship:

$$\sigma_f = \frac{3PL}{4bh^2} \quad (1)$$

where  $P$  is the applied load and  $L$  is the distance between the outer-pair of loading cylinders (shown in Figure 5b) and is set by the geometry of the apparatus to be  $L = 254$  mm.

We used two different loading procedures, as we did earlier in our study of S2 freshwater ice. Type I loading was a completely reversed stress cycle with constant stress amplitude and mean stress of zero. Type II was similar to Type I but incorporated an increasing multi-level (or step-level) stress amplitude. This second type of loading essentially consisted of several Type I steps of increasing stress amplitudes. In the present study for stress amplitudes below 0.7 MPa we used Type I loading. To cycle ice samples at stress amplitudes above 0.7 MPa, we first pre-conditioned specimens through step-loading Type II procedure at progressively higher stress amplitude levels, i.e. we cycled specimens for ~300 times at each of the following stress amplitudes: 0.7, 0.75, 0.8, 0.85 MPa and so on either until failure occurred or until a specific value of stress amplitude set by the operator (see Iliescu et al. (2017) and Murdza et al. (2018) for details). To change stress amplitude the loading was stopped for ~15 sec to change settings. After pre-conditioning, the specimens were cyclically loaded according Type I loading at least 300 times and generally for ~2000 times, since no change in strength was observed beyond a few hundred cycles (see below).

Figure 6 shows measurements of load and of displacement versus time at the beginning and near the end of cycling before specimen failure of a lower-salinity specimen (3.0±0.9 ppt). The measurements detected no softening. According to Bažant et al. (1984) softening is a decline of stress at increasing strain or, in our case, an increase of strain during cycling at constant stress amplitude during the tests). The absence of detectable softening

176 during cycling of the saline ice is reminiscent of the absence of softening during the cycling of freshwater ice  
177 (Iliescu et al., 2017; Murdza et al., 2020b).

### 178 3. Results and Observations

#### 179 3.1. Flexural strength of non-cycled ice

180 The flexural strength of non-cycled saline ice of both salinities was measured at -10 °C and at a nominal  
181 outer-fiber center-point displacement of 0.1 mm s<sup>-1</sup>. The results are listed in

182  
183

184 Table 2. Failure more often occurred at random locations between the two inner loading cylinders and less  
185 often either below or slightly outside the loading cylinders. The reason for the latter location was the presence prior  
186 to testing of a significant concentration of whitish features at loading cylinders which served as stress concentrators  
187 and along which the failure ultimately occurred (similar to Figure 4). The average and standard deviation of the  
188 measured flexural strength of saline ice of lower salinity (3.0±0.9 ppt) are 0.96±0.13 MPa. The strength of the lower  
189 salinity ice did not correlate systematically with the depth of the parent puck from which ice beams were prepared.  
190 The measured strength compares favorably with the value of 0.85±0.20 MPa reported by Timco and O'Brien (1994)  
191 for sea ice of similar salinity, as can be seen in Figure 7. Brine volume fraction  $v_b$  was calculated according to  
192 Frankenstein and Garner (1967):

193

$$v_b = 0.001 * S \left( \frac{49.185}{|T|} + 0.532 \right), \quad (2)$$

194

195 where  $T$  is temperature in degrees Celsius between -0.5 °C and -22.9 °C and  $S$  is melt-water salinity (in ppt) of the  
196 ice.

197

198 The average and standard deviation of the measured flexural strength of saline ice of higher salinity  
199 (5.9±0.6 ppt) are 0.98±0.36 MPa. The measured values (Figure 7) deviate slightly towards higher values compared  
200 to the data of Timco and O'Brien (1994), although scatter is significantly greater than is the scatter in the strength of  
201 the ice of lower salinity (3.0±0.9 ppt). This may be explained by the greater degree of interconnectivity of brine  
202 pockets at the bottom of an ice puck (discussed above and shown in Figures 3 and 4). Indeed, the flexural strength of  
203 the higher-salinity specimens appears to depend on the depth of ice from which beams were prepared, Table 2. This  
204 result shows how much the strength of ice is sensitive to flaws and defects. Given that larger bodies usually contain  
205 larger defects, the flexural strength of sea ice on the medium and large scale, in the field (Karulina et al., 2019) for  
206 instance, is expected to be lower than on the smaller scale of the present experiments.

207

208 We also compare our measurements of flexural strength with the tensile strength of sea ice. For this  
209 purpose, and as we did in our previous work on freshwater ice (Iliescu et al., 2017; Murdza et al., 2020b), flexural  
210 strength is divided by 1.7 (Ashby and Jones, 2012). This factor reflects the fact that the volume of the material  
211 which is subjected to the highest stress in bending is smaller than in uniaxial tension; thus, the largest defect which  
212 governs the failure may not be near the surface of a bent specimen. Upon dividing the flexural strength of the non-  
213 cycled saline ice of lower salinity by 1.7, we found the average across-column tensile strength from our experiments  
214 to be  $0.96 \pm 0.13 \text{ MPa} / 1.7 = 0.56 \pm 0.08 \text{ MPa}$ . This value compares favorably with the values  $0.56 \pm 0.06 \text{ MPa}$  and  
215  $0.63 \pm 0.12 \text{ MPa}$  reported by Richter-Menge and Jones (1993) for the tensile strength of columnar-grained first-year  
216 sea ice of  $4.1 \pm 0.3$  ppt salinity loaded uniaxially across the columns at a temperature of  $-10 \text{ }^\circ\text{C}$  and strain rates of  $10^{-5}$   
217 and  $10^{-3} \text{ s}^{-1}$ . Recall that in the present experiments the outer-fiber strain rate was about  $1.4 \times 10^{-4} \text{ s}^{-1}$  which is within  
218 the range reported by Richter-Menge and Jones (1993). This agreement between direct and indirect measurements of  
219 tensile strength lends confidence that our lab-grown saline ice is a reasonably faithful analogue of natural sea ice.

### 220 **3.2. Flexural strength versus number of reversed cycles under constant low stress amplitude**

221 To determine whether there is a relationship between flexural strength and number of cycles imposed under  
222 a constant low stress amplitude, we performed via Type-I loading a series of experiments on saline ice of lower  
223 salinity ( $3.0 \pm 0.9$  ppt) at  $-10 \text{ }^\circ\text{C}$  at an outer-fiber center-point displacement rate of  $0.1 \text{ mm s}^{-1}$  at a low stress  
224 amplitude of  $0.35 \text{ MPa}$ ; i.e., at an amplitude less than one-half the flexural strength of non-cycled ice. Figure 8  
225 shows the results. The number of cycles varied from about 100 to 14000. The average strength and standard  
226 deviation of all data from Figure 8 are  $0.96 \pm 0.23 \text{ MPa}$ . As noted above the strength and standard deviation of non-  
227 cycled ice are  $0.96 \pm 0.13 \text{ MPa}$ . In other words, no strengthening was detected upon cycling up to 14000 times at a  
228 stress amplitude of  $0.35 \text{ MPa}$ . For freshwater ice (Murdza et al., 2020b), we found that once the number of cycles at  
229 a given low stress amplitude exceeded 300, the number of cycles had no significant effect on the flexural strength,  
230 implying that a kind of saturation of strength developed. Given that result and the new results for saline ice, we  
231 followed the practice in the present study of cycling more than 300 times, often as many as 2000 times, before  
232 bending the ice to failure.

### 233 **3.3. Flexural strength versus stress amplitude**

234 The flexural strength increases with stress amplitude. Figure 9 shows measurements obtained from saline  
235 ice of both salinities cycled at  $-10 \text{ }^\circ\text{C}$  at an outer-fiber displacement rate of  $0.1 \text{ mm s}^{-1}$ . For comparison, data from  
236 laboratory grown freshwater ice (Murdza et al., 2020b) of S2 character and from lake ice of the same character  
237 (Murdza et al., 2020a) are also shown. The relationship between the flexural strength,  $\sigma_{fc}$  and cycled stress  
238 amplitude,  $\sigma_a$ , for saline ice appears to be a linear one and, within experimental scatter, to have essentially the same  
239 sensitivity to stress amplitude as freshwater ice; namely:

240

$$\sigma_{fc} = \sigma_{f0} + k\sigma_a , \quad (3)$$

241  
242 where  $k = 0.68$  is a constant. For freshwater ice the non-cycled flexural strength is  $\sigma_{f0} = 1.75$  MPa compared with  
243  $\sigma_{f0} = 0.96$  MPa for the saline ice. There is, perhaps, in Figure 9 a hint that for saline ice there is a threshold of  
244 about 0.4 MPa that must be exceeded to detect strengthening. Interestingly, this apparent threshold is similar in  
245 magnitude to the stress that marks the onset of significant AE activity under cyclic loading of sea ice cores (Cole  
246 and Dempsey, 2006). Although saline ice is weaker than freshwater ice, it appears that upon cycling its strength  
247 increases at the same rate as freshwater ice.

248  
249 Although the rate of strengthening with stress amplitude appears to be the same for saline ice and freshwater  
250 ice, the maximum increase in strength in the case of saline ice of lower salinity ( $3.0 \pm 0.9$  ppt) is significantly lower.  
251 We were able to strengthen saline ice by about 50% of the non-cycled strength compared with about 100% for  
252 freshwater ice (Murda et al., 2020b). Another point is that we almost were not able to cycle specimens at stress  
253 amplitudes greater than the flexural strength of non-cycled material, whereas in the case of freshwater ice we were  
254 able to cycle at stress amplitudes significantly greater than flexural strength of non-cycled ice. Indeed, the maximum  
255 cycled stress amplitude we were able to reach in the case of saline ice of lower salinity ( $3.0 \pm 0.9$  ppt) during all tests  
256 was 1.1 MPa, which is not statistically different from the non-cycled flexural strength of  $0.96 \pm 0.13$  MPa.

257  
258 For saline ice of lower salinity ( $3.0 \pm 0.9$  ppt), there is no evidence that the flexural strength of both non-  
259 cycled and cycled ice is significantly affected by the depth of ice from which ice beams were harvested. For saline  
260 ice of higher salinity ( $5.9 \pm 0.6$  ppt), however, the flexural strength of both non-cycled and cycled ice appears to  
261 depend on the depth of ice from which beams were prepared, Figure 10. Indeed, the flexural strength of specimens  
262 from the bottom and from the top of an ice puck of higher salinity ( $5.9 \pm 0.6$  ppt) differs by  $\sim 3$  times ( $\sim 0.4$  MPa vs  
263  $\sim 1.4$  MPa).

### 264 **3.4. Fatigue behavior**

265 Although the specimens from which the data in Figure 9 were obtained did not fail during cycling, other  
266 specimens cycled under similar conditions did fail while being cycled. Results from such tests (on of saline ice of  
267 lower salinity ( $3.0 \pm 0.9$  ppt) at  $-10^\circ\text{C}$  and  $0.1 \text{ mm s}^{-1}$  outer-fiber displacement rate) allowed us to construct S-N  
268 fatigue curve, shown in Figure 11. The number of cycles here is the number of cycles to failure during cycling at  
269 the last stress amplitude level and not the total number of cycles. At most the S-N curve showed only a weak  
270 systematic dependence of the number of cycles to failure on stress amplitude. Indeed, for the same stress amplitude  
271 of  $\sim 0.9$  MPa, fatigue failure occurred after as few as  $<10$  cycles and after as many as a few thousand cycles.  
272 Statistical analyses to test the hypothesis that the slope in Figure 11 is zero resulted in a p-value equal  $\sim 0.06$ .  
273 Therefore, there is only a marginally significant effect of number of cycles on the stress at which failure occurred.  
274 We attribute this variability in fatigue life to the variability in microstructure from specimen to specimen.



275

276 That said, a note of caution is appropriate. The data in Figure 11 should not be viewed as fatigue data in the  
277 usual sense; i.e., in the way such data are viewed when obtained from other materials (e.g., metals and alloys) that  
278 exhibit classical fatigue behavior. In those cases, before cycling, all specimens are assumed to have the same  
279 thermal-mechanical history. That was not the case here for the saline ice, as most of the samples were pre-  
280 conditioned according to Type II procedure before they were cycled at the last stress level where they failed while  
281 cycling. In other words, in order to get fatigue failure, we were increasing stress amplitude by small increments of  
282 ~0.05 MPa and allowed a sufficient number of cycles at each stress level (~500-1000) before we reached a fatigue  
283 failure.

284

285 The question to address here is why we did not obtain a classical S-N curve? We suggest that the classical  
286 mechanism of fatigue, i.e. accumulation of damage, is not in play in our tests and some other process is controlling  
287 fatigue life.

### 288 **3.5 Microstructural observations of samples after fatigue failure**

289 In an attempt to reveal deformation damage in the form of microcracks, we examined using thin-section  
290 optical microscopy (up to 50x magnification) the microstructure of specimens of the lower salinity ice ( $3.0 \pm 0.9$  ppt)  
291 after they had failed during cycling; i.e., failed in fatigue. Three thin sections were prepared from four specimens in  
292 order to ensure a greater probability of observing microcracks growing from brine pockets or brine channels, should  
293 they be present. The plane of the thin section was parallel to the long axis of the columnar grains and parallel to the  
294 direction of the greater normal stress. This plane was taken as the best plane to observe possible cracks. Thin  
295 sections were observed using non-polarized light. We found no evidence of microcracks starting from brine pockets  
296 or from other defects. In fact, we found no microcracks at all. It appears, therefore, that slow crack growth is not a  
297 significant contribution to the fatigue life of the beams of the laboratory-grown saline ice that we studied.

### 298 **3.6. Acoustic emissions**

299 Acoustic emissions (AE) during repetitive loading of ice have been previously recorded and analyzed in  
300 laboratory and in situ (Langhorne and Haskell, 1996), (Cole and Dempsey, 2006, 2004; Lishman et al., 2020;  
301 Murdza et al., 2020b). Langhorne and Haskell (1996) suggested that the emissions originate either from dislocation  
302 breakaway or from microcracking associated with dislocation motion.

303

304 In contrast to freshwater ice, where no sound was detected until failure (Murdza et al., 2020b), continuous  
305 emission was detected while cycling at constant stress amplitude. Figure 12 shows the cumulative acoustic  
306 emissions, or “hits”, as a function of time for ice that was cycled reversely at a constant stress amplitude of 0.5 MPa.  
307 As can be seen, the hit rate (or hits per unit time), which is the slope of the curve in Figure 12, is about the same for  
308 the duration of the experiment.

309

310 Interestingly, the hit rate depends on stress amplitude during cycling. Figure 13 shows this behavior . The  
311 greater is the stress amplitude, the greater is the hit rate. However, during cycling below about 0.2 MPa no hits were  
312 detected.

313

314 Figure 13 also indicates that the hit rate is independent of the sequence of different stress amplitudes. The  
315 numbers in Figure 13 show the order of cycling at different stress amplitudes; i.e., firstly we cycled ice at higher  
316 stress amplitudes (0.5-0.8 MPa), then at lower stress amplitudes (0.2-0.4 MPa). The results showed an increase in  
317 the hit rate as stress amplitude increases, regardless of the sequence of cycling.

#### 318 **4. Discussion**

319 The results obtained from the experiments described in this paper show that the flexural strength of saline  
320 ice can be increased upon reversed cyclic loading. Therefore, the same set of questions as for the freshwater ice  
321 should be addressed here, i.e.: What governs the flexural strength of saline ice? Does crack propagation or crack  
322 nucleation control the tensile strength? First of all, to understand the behavior of saline ice, it is important to  
323 recognize that flexural strength in the present experiments is governed by the tensile strength, although greater by a  
324 factor of about 1.7 (Ashby and Jones, 2012). Secondly, the apparent absence of remnant microcracks within the two  
325 parts of broken samples (Section 3.5) indicates that crack nucleation controls the flexural strength, just as it appears  
326 to do for freshwater ice. Indeed, this seems reasonable given the fact that freshwater ice comprises of ~95% by  
327 volume of the saline ice we studied. Within the freshwater component, there is almost no solubility of salts (Weeks  
328 and Ackley, 1986). The remainder of the saline ice is a mixture of air and brine. As was shown earlier, the  
329 microstructure of saline ice that we grew is closely similar to the microstructure of sea ice. Pores lower the saline ice  
330 strength (Sammis and Ashby, 1986). However, the behavior of S2 saline ice under cyclic loading is essentially the  
331 same as the behavior of S2 freshwater ice (Murda et al., 2020b), i.e. its strength increases at the same rate as  
332 freshwater ice upon cycling under a given amplitude of the outer fiber stress. Hence, it is reasonable to assume that  
333 the strengthening mechanism for the saline ice is similar to that for the freshwater ice. In our earlier work (Murda  
334 et al., 2020b) we proposed that strengthening might be due to the development of an internal back stress that  
335 originates from either dislocation pileups or grain boundary sliding. However, one reviewer suggested the  
336 possibility of a different strengthening mechanism. Due to the inherent weakness of the saline ice microstructure, the  
337 microstructural stress relief may occur through localized damage via microcracking mentioned above. More  
338 research, however, is needed to examine this hypothesis.

339

340 The maximum degree of strengthening in the case of saline ice is significantly lower than that for the  
341 freshwater ice, although the slopes of the two data sets (rate of strength increase with increasing cyclic amplitude) in  
342 Figure 9 are nearly equivalent. That difference may be explained by the structure of saline ice which limits  
343 maximum possible strengthening. Given the significantly greater number of stress concentrators in saline ice, such  
344 as brine pockets and channels, the propensity for failure during cycling is greater in saline ice (Sammis and Ashby,

345 1986), thereby limiting the development of the back stress. Indeed, in the present study failure of specimens during  
346 cycling occurred more frequently than in the study on freshwater ice (Murdza et al., 2020b).

347  
348 Flexural experiments conducted on saline ice of higher salinity ( $5.9\pm 0.6$  ppt) showed the importance of  
349 brine features. Samples that were manufactured from the bottom of the ice puck were characterized by more  
350 frequent whitish interconnected features (taken to be interconnected brine pockets) that often were the path for easy  
351 crack propagation. Often samples were so weak that they failed before testing simply by handling. Interestingly,  
352 there were no interconnected features in samples prepared from the top of an ice puck, which resulted in a difference  
353 of more than a factor of three in strength between samples from top and bottom. Samples produced from saline ice  
354 of lower salinity ( $3.0\pm 0.9$  ppt) also had whitish features; however, these features were spread more uniformly (on a  
355 macroscopic scale) across the sample, resulting in little difference in strength between the bottom and top samples.

356  
357 It is worth noting again that a significantly greater fraction of saline ice samples failed in fatigue while pre-  
358 conditioning compared with freshwater ice. This may be explained by the fact that freshwater ice was essentially  
359 free from pores, brine pockets and other defects. Based on this observation, it appears that crack growth is not a  
360 significant contribution to the fatigue life of saline ice under the conditions of our experiments.

361  
362 On the origin of the acoustic emissions, there are at least four possible sources of the noise detected. One is  
363 from microcracking. We imagine that microcracks form in regions of mechanical weakness which results in  
364 accumulation of damage that we detected via the AE method. Specifically, the brine drainage whitish features  
365 discussed above in the test specimens constitute regions of high porosity and thus provide favorable sites for the  
366 concentration of such damage. Failure may occur when one of these sites can no longer support the applied stress  
367 and a microcrack emerges from the damage zone and propagates. It is possible that newly formed microcracks are  
368 stable until a critical length is reached (Cannon et al., 1990; Schulson et al., 1991), at which point the crack growth  
369 ensues. The reason that microcracks were not observed under the optical microscope may be because they filled up  
370 with liquid brine upon formation which results in a loss of contrast. A second possible explanation for the acoustic  
371 emissions is the motion and friction of very fine particles of ice which may have been entrapped inside brine  
372 drainage features, as mentioned above. A third possibility is microcracking along grain boundaries due to grain  
373 boundary sliding (Elvin and Shyam Sunder, 1996; Goldsby and Kohlstedt, 1997; Mulmule and Dempsey, 1997;  
374 Schulson et al., 1997; Weiss and Schulson, 2000). A fourth possible explanation consistent with the non-history  
375 dependence of the hit rate (Figure 13) is a kind of water-hammer effect in which brine entrapped within pockets  
376 impacts the wall, first in one direction and then another. None of these possibilities can be evaluated based upon the  
377 limits of the present observations. We refrain, therefore, from further speculation on this point.

378  
379 Returning to the observations noted in the Introduction, and to the results obtained from imposed, in situ  
380 cyclic loading experiments on sea ice beams by (Bond and Langhorne, 1997; Haskell et al., 1996; Langhorne et al.,  
381 1998, 1999), the question is: Why does ice fail in the field under wave action and under imposed cyclic loading, but

382 strengthen upon cycling in our experiments in the laboratory? Although we do not know the process through which  
383 the ice sheet failed in the field, we expect that there are many micro and macro cracks in natural sea ice. Indeed,  
384 thermally-induced tensile stresses can induce thermal cracking in floating ice sheets (Evans and Untersteiner, 1971).  
385 Therefore, our sense is that the difference in ice behavior under cyclic loading in situ in the field (Bond and  
386 Langhorne, 1997; Langhorne et al., 1998) and in the laboratory in the present study is due to other types of defects  
387 other than brine channels and pockets that are generated in the field as a result of thermo-mechanical history of ice.

## 388 **5. Conclusions**

389 From new, systematic experiments on the flexural strength of sub-meter sized beams of S2 columnar-  
390 grained saline ice stressed principally across the columns through reversed cyclic loading at a temperature of -10 °C  
391 and frequencies in the range from 0.1 to 0.6 Hz, it is concluded that:

- 392 (i) The flexural strength of saline ice can be increased upon reversed cyclic loading by as much as 1.5 times.
- 393 (ii) The flexural strength of ice subsequent to cycling scales linearly with the amplitude of the outer-fiber  
394 stress.
- 395 (iii) The fatigue life of saline ice is erratic and does not obey classical S-N behavior.
- 396 (iv) Crack growth is not a significant contribution to the fatigue life of saline ice.
- 397 (v) There is high variability in structure and strength through the thickness of a saline ice puck of higher  
398 salinity ( $5.9 \pm 0.6$  ppt).
- 399 (vi) Given the lack of definitive proof of the underlying failure mechanism in saline ice, the increase in flexural  
400 strength of freshwater ice and saline ice attributable to pre-failure load cycling is roughly equivalent.
- 401 (vii) Acoustic emission hit rate during cycling at a constant stress amplitude is about constant.
- 402 (viii) Acoustic emission hit rate during cycling increases with an increase of stress amplitude of cycling.

## 403 **Acknowledgements**

404 We acknowledge helpful discussions/communications with Prof. Harold Frost, Dr. Robert Gagnon, and  
405 Dr. Daniel Iliescu. We acknowledge thoughtful and helpful critical comments from two anonymous reviewers. This  
406 work was supported by the US Department of the Interior-Bureau of Safety and Environmental Enforcement  
407 (BSEE), contract no. E16PC00005 and by National Science Foundation (FAIN 1947-107).

408  
409 **Author contributions:** AM, ES and CR designed the experiments and AM carried them out. AM prepared the  
410 manuscript with contributions from all co-authors.

411

412 **Competing interests:** The authors declare that they have no conflict of interest.

413 **References**

- 414 Ashby, M. M. and Jones, D. R. H.: Engineering Materials 1: An Introduction to Properties, Applications and  
415 Design., 2012.
- 416 Asplin, M. G., Galley, R., Barber, D. G. and Prinsenber, S.: Fracture of summer perennial sea ice by ocean swell as  
417 a result of Arctic storms, *J. Geophys. Res. Ocean.*, 117(6), 1–12, doi:10.1029/2011JC007221, 2012.
- 418 Bathias, C. and Pineau, A.: *Fatigue of Materials and Structures*, edited by C. Bathias and A. Pineau, John Wiley &  
419 Sons, Inc., Hoboken, NJ, USA., 2013.
- 420 Bažant, Z. P., Belytschko, T. B. and Chang, T.: Continuum Theory for Strain-Softening, *J. Eng. Mech.*, 110(12),  
421 1666–1692, doi:10.1061/(asce)0733-9399(1984)110:12(1666), 1984.
- 422 Bond, P. E. and Langhorne, P. J.: Fatigue behavior of cantilever beams of saline ice, *J. Cold Reg. Eng.*, 11(2), 99–  
423 112, doi:10.1061/(ASCE)0887-381X(1997)11:2(99), 1997.
- 424 Broek, D.: *Elementary engineering fracture mechanics*, 1st ed., Springer, Dordrecht., 1986.
- 425 Cannon, N. P., Schulson, E. M., Smith, T. R. and Frost, H. J.: Wing cracks and brittle compressive fracture, *Acta*  
426 *Metall. Mater.*, 38(10), 1955–1962, doi:10.1016/0956-7151(90)90307-3, 1990.
- 427 Cole, D. and Dempsey, J.: Laboratory observations of acoustic emissions from antarctic first-year sea ice cores  
428 under cyclic loading, in 18th International POAC Conference, p. Vol 3, 1083-1092., 2006.
- 429 Cole, D. M.: Reversed direct-stress testing of ice: Initial experimental results and analysis, *Cold Reg. Sci. Technol.*,  
430 18(3), 303–321, doi:10.1016/0165-232X(90)90027-T, 1990.
- 431 Cole, D. M.: A model for the anelastic straining of saline ice subjected to cyclic loading, *Philos. Mag. A*, 72(1),  
432 231–248, doi:10.1080/01418619508239592, 1995.
- 433 Cole, D. M.: Modeling the cyclic loading response of sea ice, *Int. J. Solids Struct.*, 35(31–32), 4067–4075,  
434 doi:10.1016/S0020-7683(97)00301-6, 1998.
- 435 Cole, D. M. and Dempsey, J. P.: In situ Sea Ice Experiments in McMurdo Sound: Cyclic Loading, Fracture, and  
436 Acoustic Emissions, *J. Cold Reg. Eng.*, 18(4), 155–174, doi:10.1061/(ASCE)0887-381X(2004)18:4(155), 2004.
- 437 Cole, D. M. and Durell, G. D.: The cyclic loading of saline ice, *Philos. Mag. A Phys. Condens. Matter, Struct.*  
438 *Defects Mech. Prop.*, 72(1), 209–229, doi:10.1080/01418619508239591, 1995.
- 439 Cole, D. M., Johnson, R. A. and Durell, G. D.: Cyclic loading and creep response of aligned first-year sea ice, *J.*  
440 *Geophys. Res. Ocean.*, 103(C10), 21751–21758, doi:10.1029/98JC01265, 1998.
- 441 Cole, D. M., Dempsey, J., Kjestveit, G., Shapiro, S., Shapiro, L. and Morley, G.: The cyclic and fracture response of  
442 sea ice in McMurdo Sound. Part I, in *Proceedings of the 16th IAHR International Symposium on Ice*, Dunedin, New  
443 Zealand., 2002.
- 444 Collins, C. O., Rogers, W. E., Marchenko, A. and Babanin, A. V.: In situ measurements of an energetic wave event  
445 in the Arctic marginal ice zone, *Geophys. Res. Lett.*, 42(6), 1863–1870, doi:10.1002/2015GL063063, 2015.
- 446 Dempsey, J., Cole, D. M., Shapiro, S., Kjestveit, G., Shapiro, L. and Morley, G.: The cyclic and fracture response of  
447 sea ice in McMurdo Sound. Part II, in *Proceedings of the 17th International Conference on Port and Ocean*  
448 *Engineering under Arctic Conditions*, Trondheim, Norway. [online] Available from:  
449 [https://www.researchgate.net/publication/303460064\\_The\\_cyclic\\_and\\_fracture\\_response\\_of\\_sea\\_ice\\_in\\_McMurdo](https://www.researchgate.net/publication/303460064_The_cyclic_and_fracture_response_of_sea_ice_in_McMurdo)

450 \_Sound\_Part\_II (Accessed 14 January 2020), 2003.

451 Elvin, A. A. and Shyam Sunder, S.: Microcracking due to grain boundary sliding in polycrystalline ice under  
452 uniaxial compression, *Acta Mater.*, 44(1), 43–56, doi:10.1016/1359-6454(95)00157-1, 1996.

453 Evans, R. J. and Untersteiner, N.: Thermal cracks in floating ice sheets, *J. Geophys. Res.*, 76(3), 694–703,  
454 doi:10.1029/JC076i003p00694, 1971.

455 Frankenstein, G. and Garner, R.: Equations for Determining the Brine Volume of Sea Ice from  $-0.5^{\circ}$  to  $-22.9^{\circ}\text{C}$ ., *J.*  
456 *Glaciol.*, 6(48), 943–944, doi:10.3189/S0022143000020244, 1967.

457 Golding, N., Snyder, S. A., Schulson, E. M. and Renshaw, C. E.: Plastic faulting in saltwater ice, *J. Glaciol.*,  
458 60(221), 447–452, doi:10.3189/2014JoG13J178, 2014.

459 Goldsby, D. L. and Kohlstedt, D. L.: Grain boundary sliding in fine-grained ice I, *Scr. Mater.*, 37(9), 1399–1406,  
460 doi:10.1016/S1359-6462(97)00246-7, 1997.

461 Gupta, V., Bergström, J. and Picu, C. R.: Effect of step-loading history and related grain-boundary fatigue in  
462 freshwater columnar ice in the brittle deformation regime, *Philos. Mag. Lett.*, 77(5), 241–247,  
463 doi:10.1080/095008398178372, 1998.

464 Haskell, T. G., Robinson, W. H. and Langhorne, P. J.: Preliminary results from fatigue tests on in situ sea ice beams,  
465 *Cold Reg. Sci. Technol.*, 24(2), 167–176, doi:10.1016/0165-232X(95)00015-4, 1996.

466 Hendrikse, H. and Metrikine, A.: Edge indentation of ice with a displacement-controlled oscillating cylindrical  
467 structure, *Cold Reg. Sci. Technol.*, 121, 100–107, doi:10.1016/j.coldregions.2015.10.013, 2016.

468 Hwang, B., Wilkinson, J., Maksym, E., Graber, H. C., Schweiger, A., Horvat, C., Perovich, D. K., Arntsen, A. E.,  
469 Stanton, T. P., Ren, J. and Wadhams, P.: Winter-to-summer transition of Arctic sea ice breakup and floe size  
470 distribution in the Beaufort Sea, *Elem Sci Anth*, 5, 40, doi:10.1525/elementa.232, 2017.

471 Iliescu, D. and Schulson, E. M.: Brittle compressive failure of ice: Monotonic versus cyclic loading, *Acta Mater.*,  
472 50(8), 2163–2172, doi:10.1016/S1359-6454(02)00060-5, 2002.

473 Iliescu, D., Murdza, A., Schulson, E. M. and Renshaw, C. E.: Strengthening ice through cyclic loading, *J. Glaciol.*,  
474 63(240), 663–669, doi:10.1017/jog.2017.32, 2017.

475 Jordaan, I. J.: Mechanics of ice–structure interaction, *Eng. Fract. Mech.*, 68(17–18), 1923–1960, doi:10.1016/S0013-  
476 7944(01)00032-7, 2001.

477 Jordaan, I. J., Xiao, J., Wells, J. and Derradji-Aouat, A.: Ice crushing and cyclic loading in compression, in 19th  
478 IAHR International Symposium on Ice, pp. 1097–1106., 2008.

479 Karulina, M., Marchenko, A., Karulin, E., Sodhi, D., Sakharov, A. and Chistyakov, P.: Full-scale flexural strength  
480 of sea ice and freshwater ice in Spitsbergen Fjords and North-West Barents Sea, *Appl. Ocean Res.*, 90,  
481 doi:10.1016/j.apor.2019.101853, 2019.

482 Kohout, A. L., Williams, M. J. M., Toyota, T., Lieser, J. and Hutchings, J.: In situ observations of wave-induced sea  
483 ice breakup, *Deep. Res. Part II Top. Stud. Oceanogr.*, 131, 22–27, doi:10.1016/j.dsr2.2015.06.010, 2016.

484 Langhorne, P. J. and Haskell, T. G.: Acoustic emission during fatigue experiments on first year sea ice, *Cold Reg.*  
485 *Sci. Technol.*, 24(3), 237–250, doi:10.1016/0165-232X(95)00021-3, 1996.

486 Langhorne, P. J., Squire, V. A., Fox, C. and Haskell, T. G.: Break-up of sea ice by ocean waves, *Ann. Glaciol.*, 27,

487 438–442, doi:10.3189/S0260305500017869, 1998.

488 Langhorne, P. J., Squire, V. A. and Haskell, T. G.: Role of fatigue in wave-induced break-up of sea ice- a review, in

489 Ice in Surface Waters: Proceedings of the 14th International Symposium on Ice, pp. 1019–1023, Rotterdam, The

490 Netherlands., 1999.

491 Langhorne, P. J., Squire, V. A., Fox, C. and Haskell, T. G.: Lifetime estimation for a land-fast ice sheet subjected to

492 ocean swell, *Ann. Glaciol.*, 33, 333–338, doi:10.3189/172756401781818419, 2001.

493 Lishman, B., Marchenko, A., Sammonds, P. and Murdza, A.: Acoustic emissions from in situ compression and

494 indentation experiments on sea ice, *Cold Reg. Sci. Technol.*, 172, 102987, doi:10.1016/j.coldregions.2019.102987,

495 2020.

496 Liu, A. K., Mollo-Christensen, E., Liu, A. K. and Mollo-Christensen, E.: Wave Propagation in a Solid Ice Pack, *J.*

497 *Phys. Oceanogr.*, 18, 1702–1712, doi:10.1175/1520-0485(1988)018<1702:WPIASI>2.0.CO;2, 1988.

498 Masterson, D.: *The Story of Offshore Arctic Engineering - Dan Masterson* - Google Books, Cambridge Scholars

499 Publishing. [online] Available from:

500 [https://books.google.com/books/about/The\\_Story\\_of\\_Offshore\\_Arctic\\_Engineering.html?id=y9N1DwAAQBAJ](https://books.google.com/books/about/The_Story_of_Offshore_Arctic_Engineering.html?id=y9N1DwAAQBAJ)

501 (Accessed 4 March 2021), 2018.

502 Michel, B. and Ramseier, R. O.: Classification of river and lake ice, *Can. Geotech. J.*, 8(1), 36–45, doi:10.1139/t71-

503 004, 1971.

504 Mulmule, S. V. and Dempsey, J. P.: Stress-Separation Curves for Saline Ice Using Fictitious Crack Model, *J. Eng.*

505 *Mech.*, 123(8), 870–877, doi:10.1061/(asce)0733-9399(1997)123:8(870), 1997.

506 Murdza, A., Schulson, E. M. and Renshaw, C. E.: Hysteretic behavior of freshwater ice under cyclic loading :

507 preliminary results, in 24th IAHR International Symposium on Ice, pp. 185–192, Vladivostok., 2018.

508 Murdza, A., Schulson, E. M. and Renshaw, C. E.: The Effect of Cyclic Loading on the Flexural Strength of

509 Columnar Freshwater Ice, in Proceedings of the 25th International Conference on Port and Ocean Engineering under

510 Arctic Conditions, Delft, Netherlands., 2019.

511 Murdza, A., Marchenko, A., Schulson, E. M. and Renshaw, C. E.: Cyclic strengthening of lake ice, *J. Glaciol.*,

512 67(261), 182–185, doi:10.1017/jog.2020.86, 2020a.

513 Murdza, A., Schulson, E. M. and Renshaw, C. E.: Strengthening of columnar-grained freshwater ice through cyclic

514 flexural loading, *J. Glaciol.*, 66(258), 556–566, doi:10.1017/jog.2020.31, 2020b.

515 O’Rourke, B. J., Jordaan, I. J., Taylor, R. S. and Gürtner, A.: Experimental investigation of oscillation of loads in ice

516 high-pressure zones, part 1: Single indenter system, *Cold Reg. Sci. Technol.*, 124, 25–39,

517 doi:10.1016/J.COLDREGIONS.2015.12.005, 2016.

518 Pistone, K., Eisenman, I. and Ramanathan, V.: Observational determination of albedo decrease caused by vanishing

519 Arctic sea ice, *Proc. Natl. Acad. Sci. U. S. A.*, 111(9), 3322–3326, doi:10.1073/pnas.1318201111, 2014.

520 Prinsenbergh, S. J. and Peterson, I. K.: Observing regional-scale pack-ice decay processes with helicopter-borne

521 sensors and moored upward-looking sonars, *Ann. Glaciol.*, 52(57), 35–42, doi:10.3189/172756411795931688,

522 2011.

523 Richter-Menge, J. A. and Jones, K. F.: The tensile strength of first-year sea ice, *J. Glaciol.*, 39(133), 609–618,

524 doi:10.3189/S0022143000016506, 1993.

525 Sammis, C. G. and Ashby, M. F.: The failure of brittle porous solids under compressive stress states, *Acta Metall.*,  
526 34(3), 511–526, doi:10.1016/0001-6160(86)90087-8, 1986.

527 Schijve, J.: *Fatigue of Structures and Materials*, 2nd ed., Springer Netherlands., 2009.

528 Schulson, E. M. and Duval, P.: *Creep and Fracture of Ice*, Cambridge University Press, Cambridge., 2009.

529 Schulson, E. M., Kuehn, G. A., Jones, D. A. and Fifolt, D. A.: The growth of wing cracks and the brittle  
530 compressive failure of ice, *Acta Metall. Mater.*, 39(11), 2651–2655, doi:10.1016/0956-7151(91)90081-B, 1991.

531 Schulson, E. M., Qi, S., Melton, J. S. and Gratz, E. T.: Across-column cracks and axial splits in S2 saline ice under  
532 compression, *J. Glaciol.*, 43(145), 411–414, doi:10.3189/s0022143000034997, 1997.

533 Shackleton, E. H.: *South: The Story of Shackleton’s Last Expedition, 1914–17*, Macmillian, USA., 1982.

534 Squire, V. A.: Of ocean waves and sea-ice revisited, *Cold Reg. Sci. Technol.*, 49(2), 110–133,  
535 doi:10.1016/j.coldregions.2007.04.007, 2007.

536 Suresh, S.: *Fatigue of Materials*, Cambridge University Press., 1998.

537 Tabata, T. and Nohguchi, Y.: Failure of Sea Ice by Repeated Compression, in *Physics and Mechanics of Ice*, pp.  
538 351–362, Springer Berlin Heidelberg, Berlin, Heidelberg., 1980.

539 Timco, G. W. and O’Brien, S.: Flexural strength equation for sea ice, *Cold Reg. Sci. Technol.*, 22(3), 285–298,  
540 doi:10.1016/0165-232X(94)90006-X, 1994.

541 Weeks, W. F.: *On Sea Ice*, University of Alaska Press., 2010.

542 Weeks, W. F. and Ackley, S. F.: The Growth, Structure, and Properties of Sea Ice, in *The Geophysics of Sea Ice*, pp.  
543 9–164, Springer US, Boston, MA., 1986.

544 Wei, M., Polojärvi, A., Cole, D. M. and Prasanna, M.: Strain response and energy dissipation of floating saline ice  
545 under cyclic compressive stress, *Cryosph.*, 14(9), 2849–2867, doi:10.5194/tc-14-2849-2020, 2020.

546 Weiss, J. and Schulson, E. M.: Grain-boundary sliding and crack nucleation in ice, *Philos. Mag. A*, 80(2), 279–300,  
547 doi:10.1080/01418610008212053, 2000.

548 Zhang, R., Wang, H., Fu, Q., Rasch, P. J. and Wang, X.: Unraveling driving forces explaining significant reduction  
549 in satellite-inferred Arctic surface albedo since the 1980s, *Proc. Natl. Acad. Sci. U. S. A.*, 116(48), 23947–23953,  
550 doi:10.1073/pnas.1915258116, 2019.

551

552

553

554

555

556

557

558

559

560



561  
562  
563  
564

**Table 1. Physical properties of as-grown saline ice.**

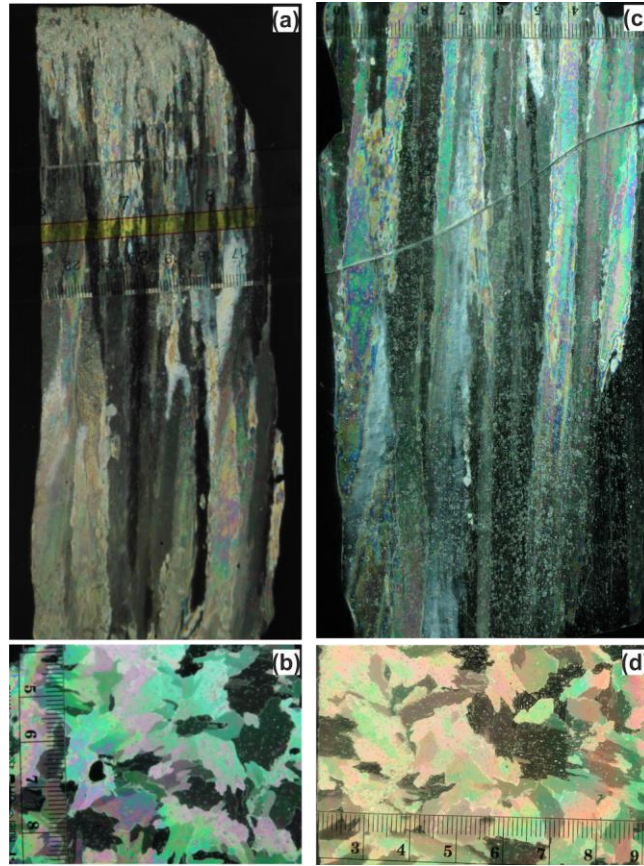
<b>Material</b>	<b>Density [kg m<sup>-3</sup>]</b>	<b>Average salinity [ppt]</b>	<b>Grain size [mm]</b>
Saline ice (lower salinity)	878±11	3.0±0.9	3.8±0.9
Saline ice (higher salinity)	897±10	5.9±0.6	3.6±1.1

565  
566  
567  
568

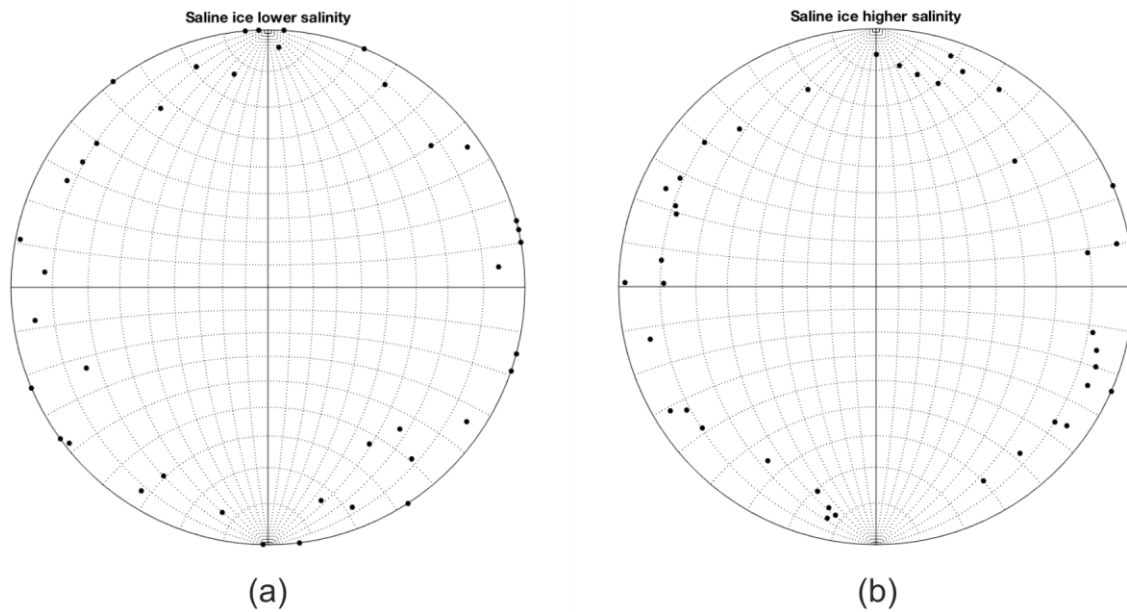
569 **Table 2. Flexural strength of non-cycled saline ice at -10°C and a displacement rate of 0.1 mm/s.**

<b>Flex strength of ice of lower salinity (3.0±0.9 ppt) [MPa]</b>	<b>Depth [cm]</b>	<b>Flex strength of ice of higher salinity (5.9±0.6 ppt) [MPa]</b>	<b>Depth [cm]</b>
1.08	—	0.45	20 – 22.5
0.86	—	0.53	17.5 – 20
1.06	—	0.62	12.5 – 15
0.96	—	0.98	7.5 – 10
0.83	17 – 21	1.17	5 – 7.5
0.75	13.5 – 17	1.26	5 – 7.5
1.08	10 – 13.5	1.26	2.5 – 5
0.97	6.5 – 10	1.44	1 – 2.5
1.09	3 – 6.5	1.17	—
Average		Average	
0.96±0.13		0.98±0.36	

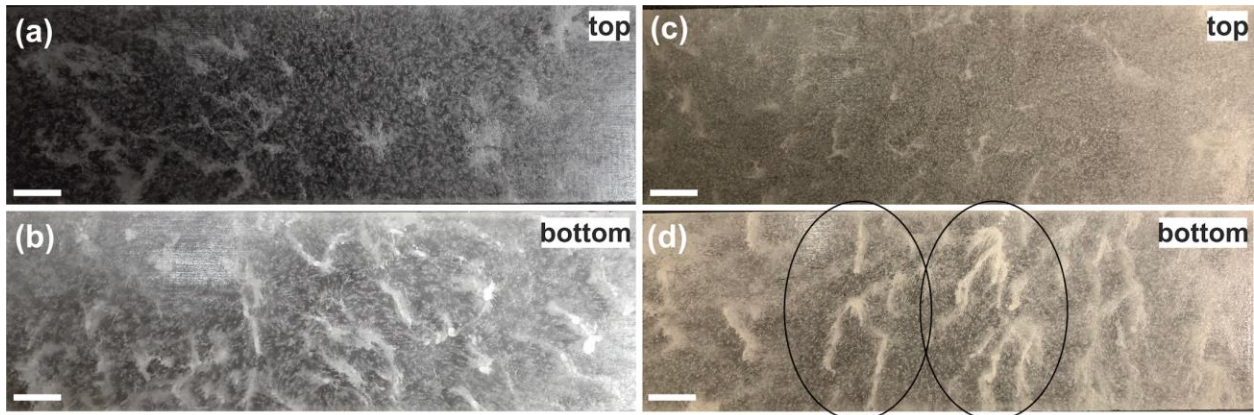
570  
571



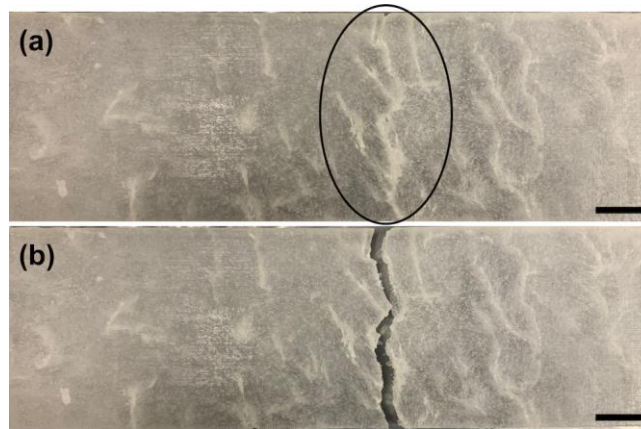
572  
 573 **Figure 1.** Photographs of a vertically-oriented (a) and a horizontally-oriented (b) thin-sections (~1mm) of columnar-  
 574 grained, saline ice of lower salinity ( $3.0 \pm 0.9$  ppt) as viewed between crossed-polarized filters; photographs of a vertically-  
 575 oriented (c) and a horizontally-oriented (d) thin-sections of saline ice of higher salinity ( $5.9 \pm 0.6$  ppt).



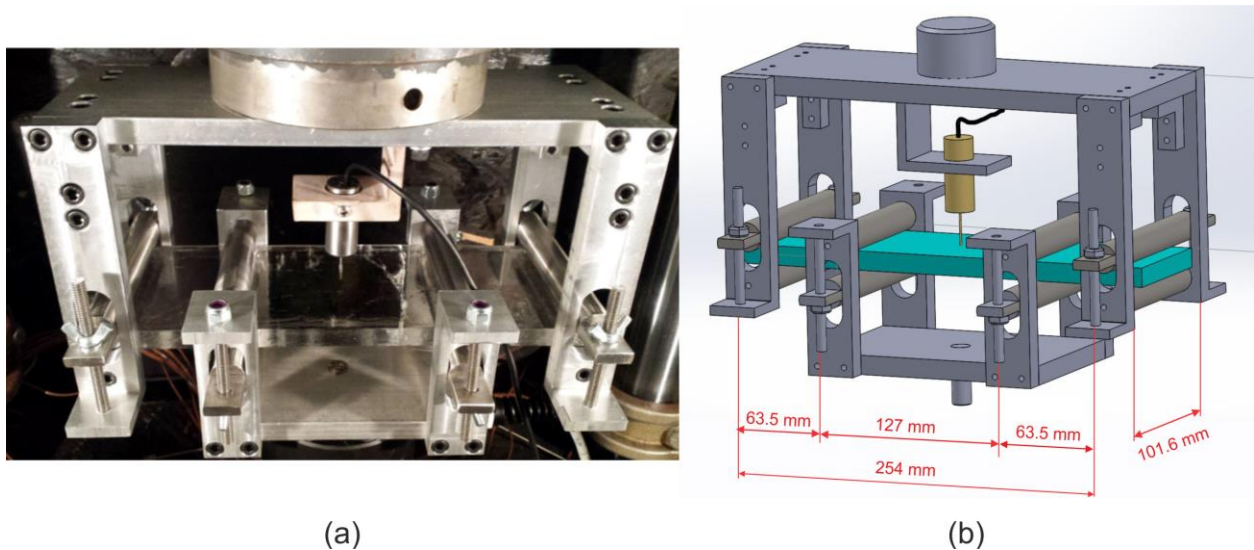
576  
 577 **Figure 2.** Stereographic projection plots of crystal c-axis {0001} orientations in saline ice of lower ( $3.0 \pm 0.9$  ppt) salinity (a)  
 578 and saline ice of higher ( $5.9 \pm 0.6$  ppt) salinity (b).



579  
580  
581  
582  
583  
 Figure 3. Photographs of saline ice samples of lower salinity ( $3.0\pm 0.9$  ppt) from the top (a) and bottom (b) of an ice block and saline ice samples of higher salinity ( $5.9\pm 0.6$  ppt) from the top (c) and bottom (d) of an ice block. The concentration of whitish features along the width of a sample in (d) is shown inside circles which is a predominant place for a crack to initiate. The columnar grains run in and out of the images. Scale bars: 20 mm.

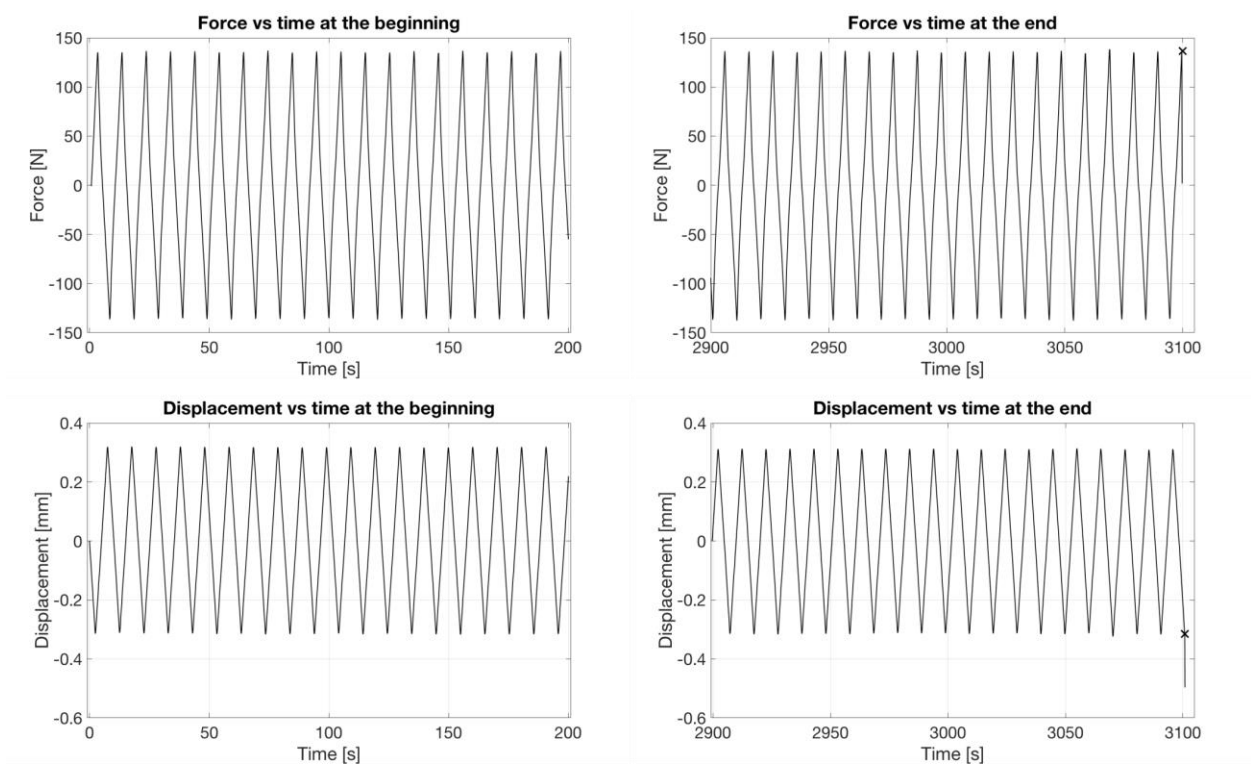


584  
585  
586  
587  
 Figure 4. Photograph of a sample from the bottom of an ice block of higher salinity ( $5.9\pm 0.6$  ppt) before cycling (a) and after (b) failure. Note a crack that propagated along whitish features in the area in (a) depicted by the circle. Scale bars: 20 mm.

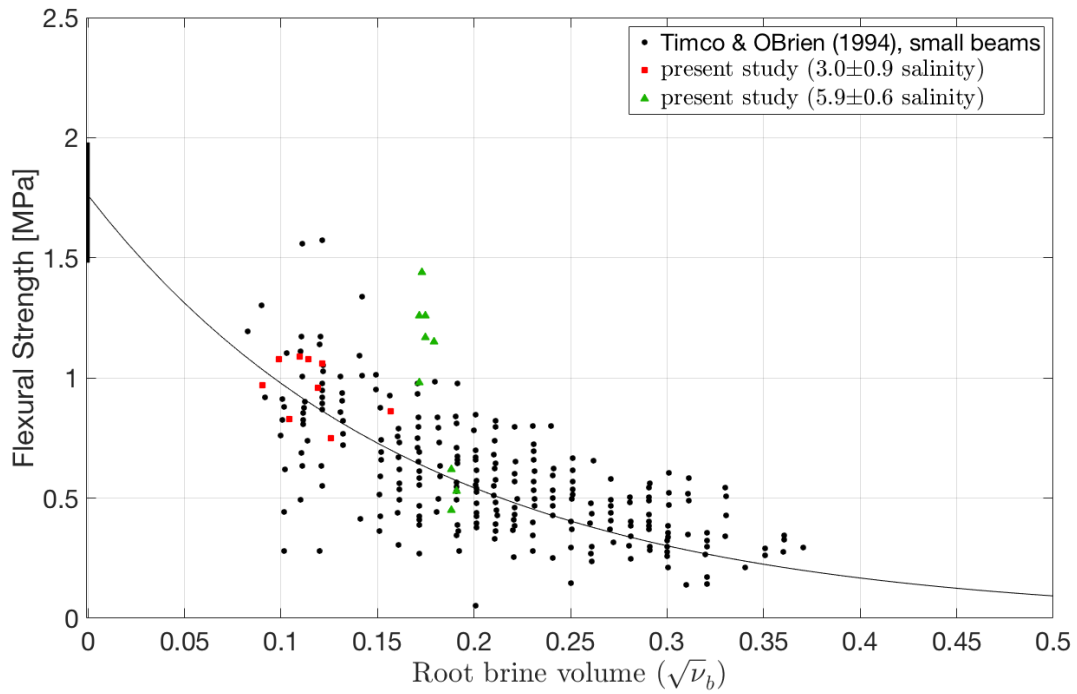


588  
589  
590  
 Figure 5. Photograph (a) and sketch (b) of the four-point bending apparatus connected to an MTS hydraulic testing system (Iliescu et al., 2017; Murdza et al., 2020b). The upper part is attached to the frame of the machine while the mobile

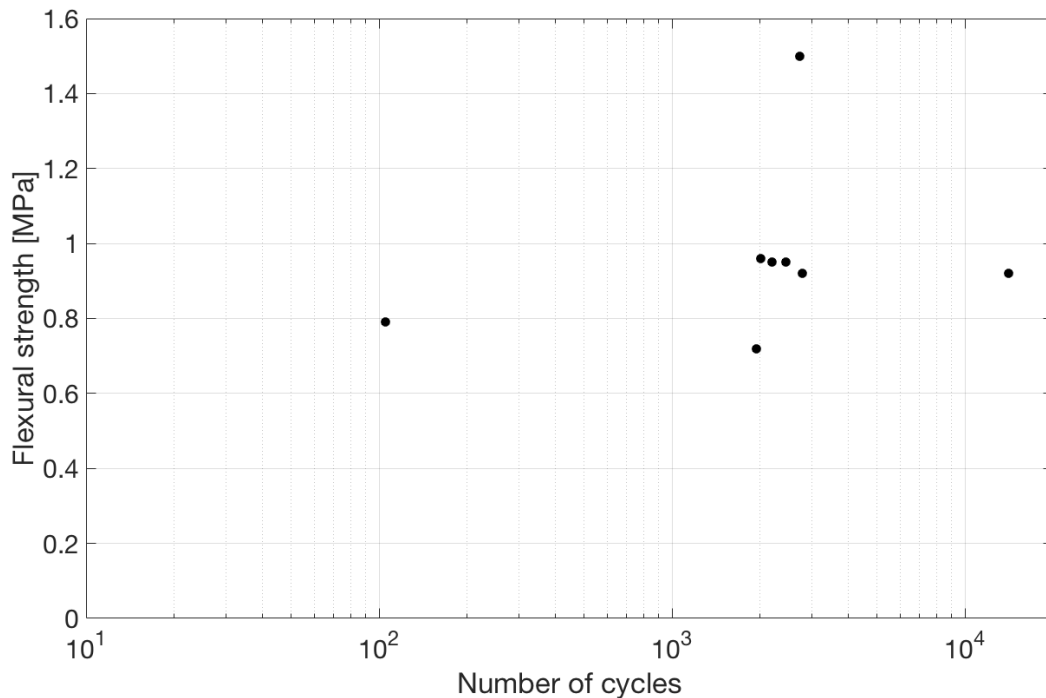
591 middle part is attached through a fatigue-rated load cell to the piston. The apparatus is made from an aluminum alloy;  
592 the loading cylinders are made from stainless steel.



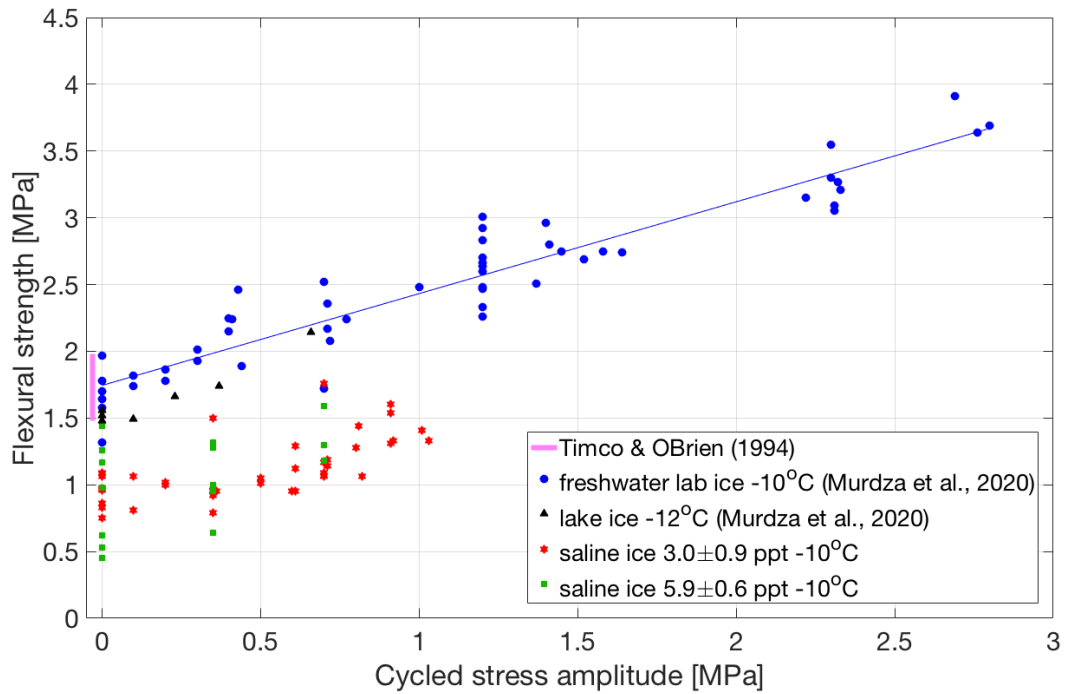
593  
594 **Figure 6. Curves of force/load and displacement vs. time for periods of 200 s near the beginning and near the end of**  
595 **cycling before fatigue failure occurred. Marker symbol “x” denotes a moment of specimen failure. Force of ~135 N**  
596 **corresponds to ~1.2 MPa.**



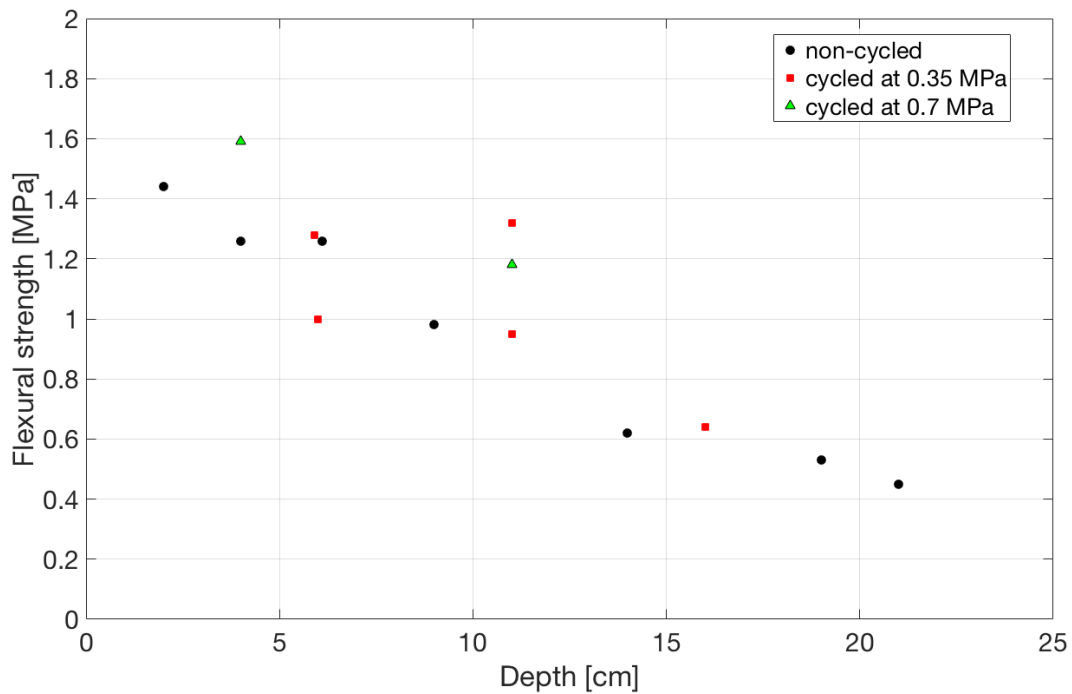
597  
 598 **Figure 7. Flexural strength of saline ice as a function of root brine volume for the ice grown in the present study and for**  
 599 **data from Timco and O'Brien (1994) for comparison.**



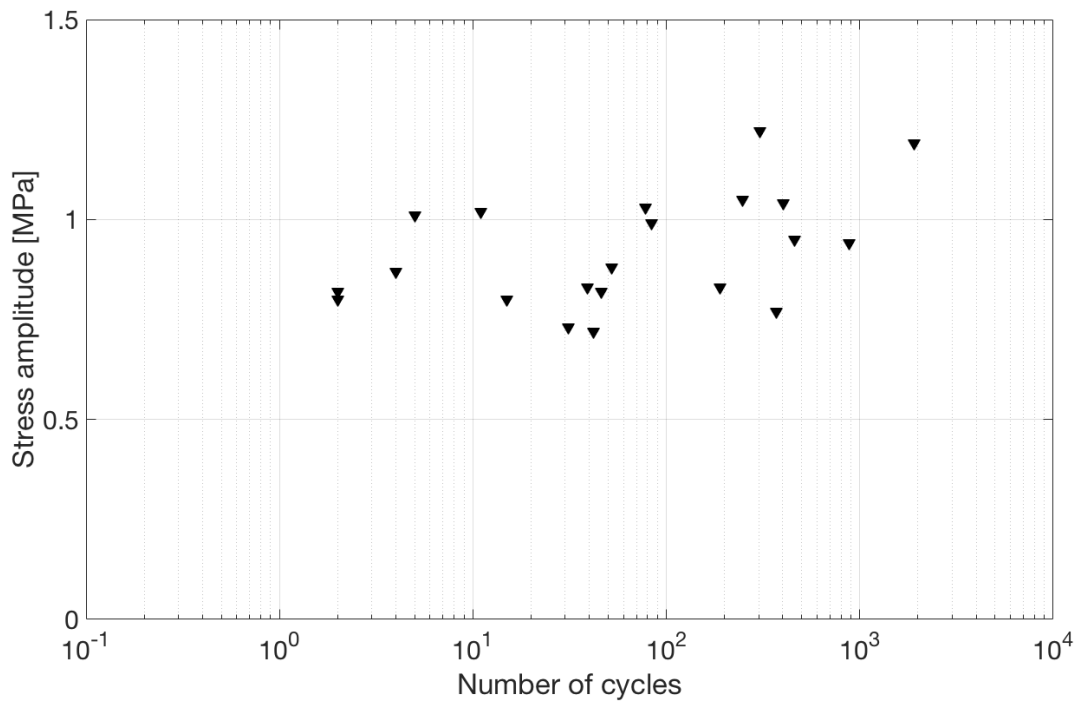
600  
 601 **Figure 8. Flexural strength and the corresponding number of cycles imposed for saline ice of lower salinity ( $3.0 \pm 0.9$ ) ppt**  
 602 **cycled at  $0.35$  MPa outer-fiber stress amplitude at  $-10$  °C and  $0.1$  mm s $^{-1}$  outer-fiber center-point displacement rate.**



603  
 604 **Figure 9. Flexural strength of freshwater ice and saline ice of lower ( $3.0\pm 0.9$  ppt) and of higher ( $5.9\pm 0.6$  ppt) salinity as a**  
 605 **function of reverse-cycled stress amplitude. Freshwater ice laboratory and lake data are taken from (Murda et al., 2020b,**  
 606 **2020a). Red five-pointed stars and green squares represent tests performed on saline ice of lower and higher salinities,**  
 607 **respectively, at  $0.1\text{ mm s}^{-1}$  and  $-10^\circ\text{C}$ . During all depicted tests the ice did not fail during cycling and was broken by**  
 608 **applying one unidirectional displacement until failure occurred.**

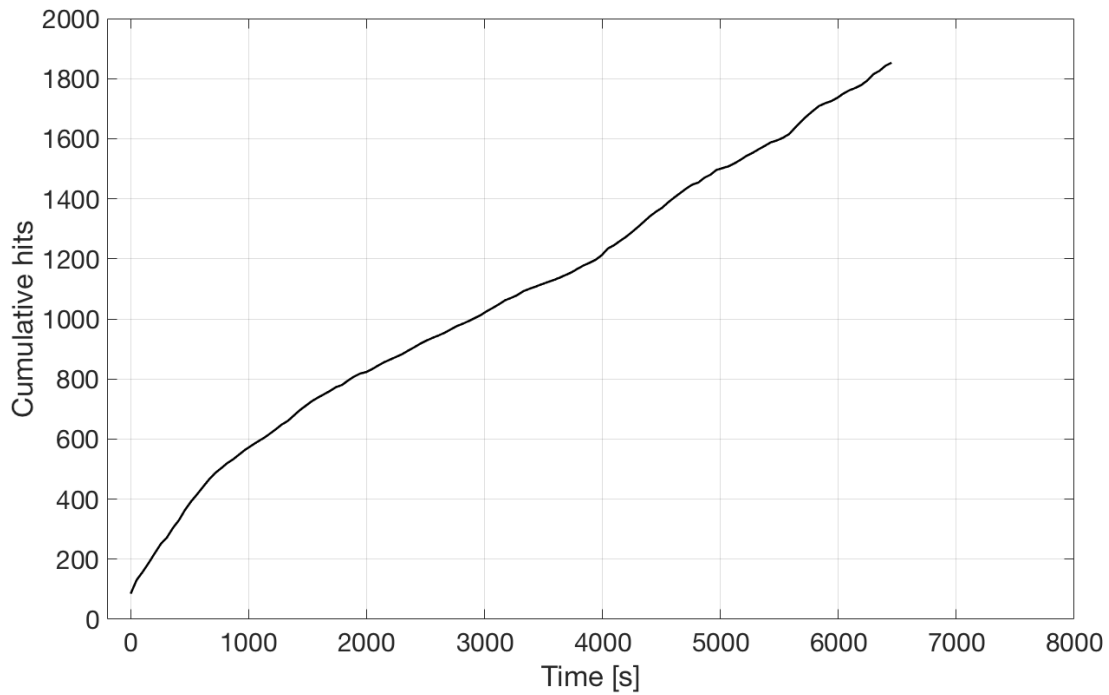


609  
 610 **Figure 10. Flexural strength as a function of position of saline ice samples of higher salinity ( $5.9\pm 0.6$  ppt) for different**  
 611 **cyclic amplitudes. The imposed number of cycles for specimens cycled at 0.35 and 0.7 MPa is  $\sim 2000$ .**

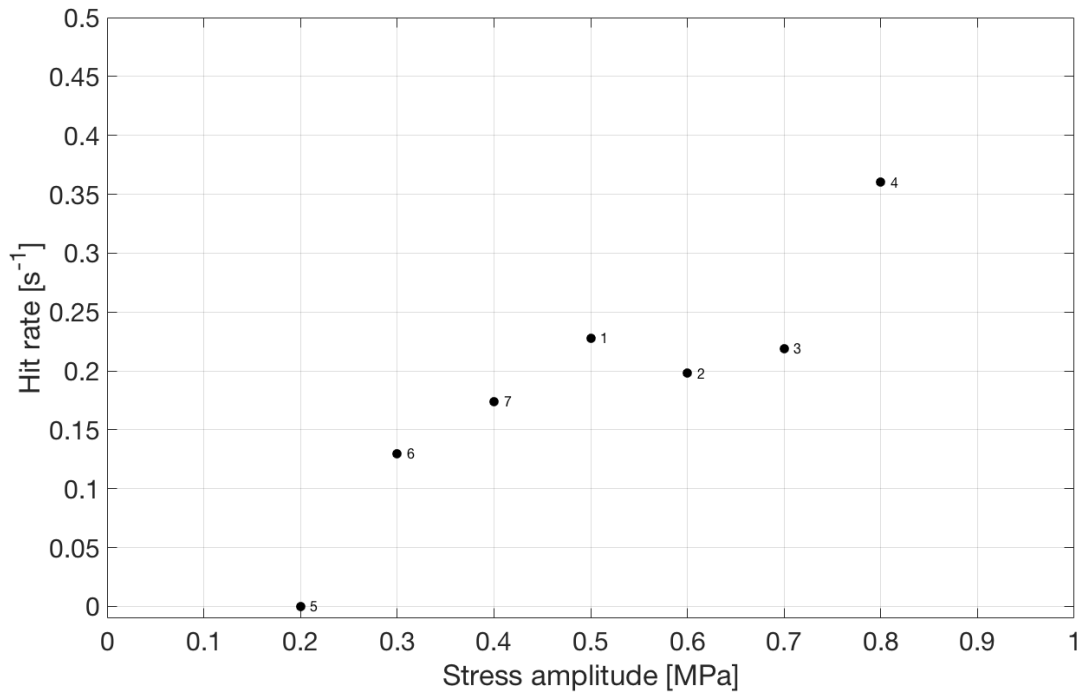


612  
 613 **Figure 11. Stress amplitude as a function of the number of cycles to fatigue fracture for saline ice of lower salinity**  
 614 **( $3.0 \pm 0.9$  ppt) tested at  $-10^\circ\text{C}$  and  $0.1 \text{ mm s}^{-1}$  outer-fiber center-point displacement rate.**

615



616  
 617 **Figure 12. Acoustic emissions (hits) against time for saline ice of lower salinity ( $3.0 \pm 0.9$  ppt), cycled at a stress amplitude**  
 618 **of  $0.5 \text{ MPa}$  at  $-10^\circ\text{C}$  at an outer-fiber displacement rate of  $0.1 \text{ mm s}^{-1}$ .**



619  
620 **Figure 13. Hit rate as a function of cycled stress amplitude for saline ice sample of lower salinity ( $3.0 \pm 0.9$  ppt). Numbers**  
621 **show the order of cycling at different stress amplitudes.**

622  
623  
624